

# Strain-induced gradient crystalline evolution mechanism of Ti-6.5Al-3.5Mo-1.5Zr-0.3Si during ultrasonic impacting and rolling process

Yu Liu<sup>1,2</sup>, Guilian Xue<sup>3</sup>, Xiaohui Zhao<sup>2,3</sup> ✉

<sup>1</sup>School of Mechanical Science and Engineering, Jilin University, Changchun, 130025, People's Republic of China

<sup>2</sup>Department of Mechanical Engineering, Politecnico di Milano, Via La Masa 1, Milan, 20156, Italy

<sup>3</sup>Key Laboratory of Automobile Materials, School of Materials Science and Engineering, Jilin University, Changchun, 130025, People's Republic of China

✉ E-mail: zhaoxiaohui@jlu.edu.cn

Published in Micro & Nano Letters; Received on 12th December 2016; Accepted on 23rd January 2017

This study investigates the gradient crystalline evolution mechanism of titanium alloy Ti-6.5Al-3.5Mo-1.5Zr-0.3Si during ultrasonic impacting and rolling process (UIRP). Microscopic observations indicated that dislocation movement is quite active at the early stage of plastic deformation, but twinning soon dominates the plastic deformation in the following long period of time. The very high energy density provided by the UIRP generates a surprisingly large number of epitaxy stacking faults despite the high energy they require. The actual atomic layers present a topological structure, facilitating the conversion between intrinsic stacking faults and epitaxy stacking faults, promoting the generation of twins, partial dislocations, and their intersection. After grains are refined to nano-scale, dislocation slip again becomes the main deformation mode. In addition, beamlike secondary  $\alpha$ -phase and laminar secondary  $\alpha$ -phase were observed precipitating in  $\beta$ -substrate. These secondary  $\alpha$ -phases could reduce the dislocation slip resistance and improve the elongation, thus contributing to improve the plasticity of alloy.

**1. Introduction:** Titanium alloys are increasingly used in many industrial fields due to their superior specific strength, good corrosion resistance and outstanding intermediate temperature performance [1–3]. To improve the performance of titanium structures, severe plastic deformation (SPD) is usually adopted to produce gradient crystalline surfaces [4–6]. Study showed that for hexagonal close-packed (hcp) metals deformation twinning occurs at the early stage of SPD, and is considered as an additional deformation mechanism to dislocation slip [7]. Dislocation-twin boundary interactions were also reported to play important roles in grain refinement, which may be a type of surface nanocrystallisation mechanism for metals with medium stacking fault energy (SFE) [8]. Titanium alloy has a medium SFE with the value of about  $300 \text{ mJ m}^{-2}$  [9]. Its hcp  $\alpha$ -phase has four independent slip systems with the main slip plane of (0001), and its body-centred cubic  $\beta$ -phase has 12 independent slip systems with the main slip plane family of {110} [10]. Though the independent slip systems of  $\alpha$ -phase are not enough to make plastic deformation, the medium SFE is conducive to produce twins and facilitates the plastic deformation. Twinning usually occurs simultaneously with stacking fault and partial dislocation slip, yet detailed research on this is rarely reported. Hence, the present work focuses on the activeness of dislocation and twinning during SPD for fully understanding surface nanocrystallisation mechanism of titanium alloy.

**2. Material and methods:** The experimental material was the as-received Ti-6.5Al-3.5Mo-1.5Zr-0.3Si with chemical composition of (in wt.%): 5.8~7.0Al, 2.8~3.8Mo, 0.8~2.0Zr, 0.25Fe, 0.20~0.35Si, 0.08C, 0.05N, 0.012H, 0.15O and balance Ti. Ultrasonic impacting and rolling process (UIRP) was adopted to prepare gradient crystalline surface. As a newly proposed surface nanocrystallisation technology, detailed description of its apparatus and working principle was reported previously [11]. In brief, the piezoelectric ceramic transducer in UIRP tool converts the electrical oscillation supplied by ultrasonic generator to ultrasonic vibration. This ultrasonic vibration is further amplified and passed to the processing head which is a rotatable cemented carbide ball mounted

in the front of UIRP tool. With the aid of numerically-controlled machine, the processing head impacts material surface in ultrasonic frequency during rolling on the entire processing area with constant pressure. The specimen was a  $100 \times 100 \times 6 \text{ mm}$  plate. Fig. 1a schematically shows the moving path of processing head.

UIRP parameters include static force of 600 N, vibration amplitude of  $10 \mu\text{m}$ , feeding rate of 3000 mm/min and stepping distance of 0.2 mm. After UIRP, a Zeiss Axio Imager A1m type of optical microscope was used to observe the cross-sectional metallographic structure. A STRESS X3000 X-ray diffractometer was used for phase testing. A JEM-2010 type of transmission electron microscopy (TEM) was employed for crystalline structure investigation. TEM samples were sliced strictly parallel to the treated surface and micro-grounded to  $30 \mu\text{m}$  in thickness, followed by low energy ion milling to complete the final foils.

**3. Results and discussion:** As observed from Fig. 1a, the microstructure in top surface is obviously smaller and denser than that in matrix, indicating that SPD occurs after UIRP. The XRD pattern in Fig. 1b confirms the fact that the experimental material contains  $\alpha$ -phase and  $\beta$ -phase.

Fig. 2 shows the TEM bright field images and corresponding selected area electron diffraction (SAED) patterns at about 150, 120 and  $90 \mu\text{m}$  below top surface. As observed from Fig. 2a, grains at the depth of  $150 \mu\text{m}$  mostly keep original size. Dislocations appear inside the grains and start to gather with certain density, indicating that plastic strain has been induced in this layer. With the increase of strain, these dislocations continue accumulating and form dislocation walls, clearly shown in Fig. 2b. These dislocation walls, which will become sub-boundaries, divide the original grains into 400–500 nm. Meanwhile, dislocations still nucleate inside substructures, illustrating the fact that dislocation movement is quite active at the early stage of plastic deformation. This is due to the medium SFE titanium possesses. Moreover, for the same reason, twinning emerges to coordinate with deformation as strain increasing, especially in  $\alpha$ -phase, as shown in Fig. 2c where a twin band links the dislocation tangles on its both sides.

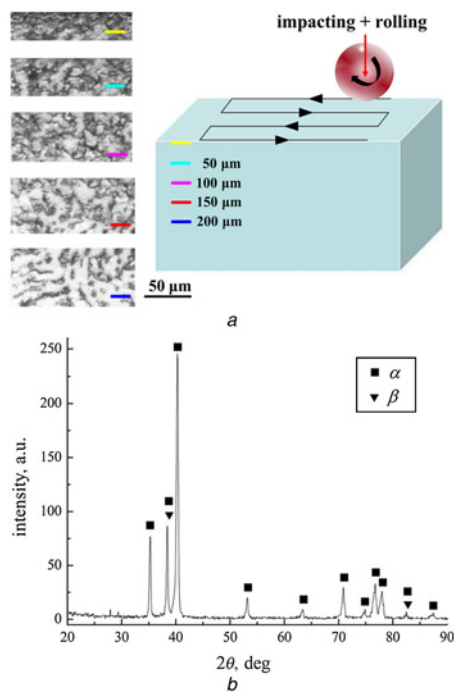


**Fig. 1** Schematic procedure of UIRP with  
*a* Metallographs of different depth and  
*b* X-ray diffraction pattern of titanium alloy after UIRP

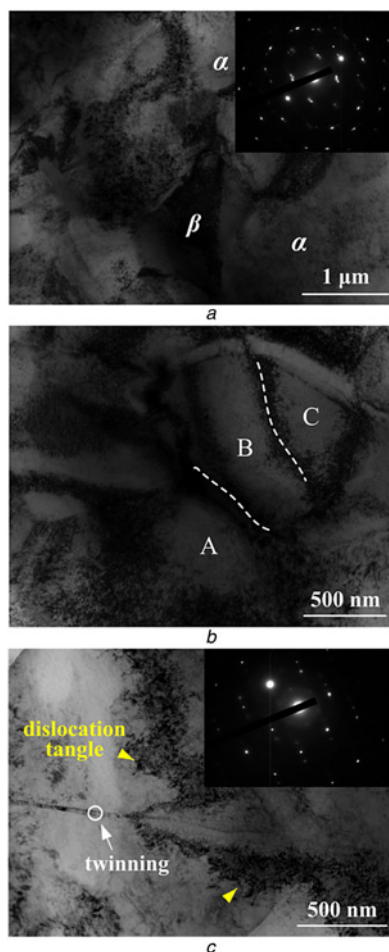


**Fig. 2** TEM bright field images and the corresponding SAED patterns at  
*a* About 150  $\mu\text{m}$ ;  
*b* About 120  $\mu\text{m}$  and  
*c* About 90  $\mu\text{m}$  below the top surface

In the middle stage of surface nanocrystallisation, twinning continues populating the microstructure. This can be reflected by the massive stacking faults (see Fig. 3*a*) which are the necessary conditions for the formation of twins. With such convenient conditions, twins are largely generated and present rhombic angulars among each other, as marked by the white arrows in Fig. 3*b* and the corresponding SAED pattern in Fig. 3*d*. By intersection, the rhombic blocks produced by these twins will further break up the original grains [12]. Fig. 3*c* shows the corresponding SAED pattern with [2-1-10] zone axis, again showing the active stacking faults in  $\alpha$ -grains. It is worth noting that the extensive stacking faults are not only observed in the selected visual area, but also found widespread in the TEM sample, demonstrating that twinning dominates the plastic deformation in this stage even though the dislocation activities still proceed. Also,  $\alpha$ -phase occupies a much higher volume fraction than  $\beta$ -phase. To make a more in-depth analysis, high resolution transmission electron microscopic (HRTEM) observation was performed with the image shown in Fig. 3*e*.

As intuitively observed in Fig. 3*e*, there are a great many of stacking faults. For clear illustration, the three types of stacking faults are labelled as  $I_1$ ,  $I_2$  and  $E$ , representing two kinds of intrinsic stacking faults and epitaxy stacking fault, respectively. Typical  $I_1$ ,  $I_2$  and  $E$  selected from Fig. 3*e* are further enlarged on the right-hand side. Though both named with intrinsic stacking fault, the  $I_1$  type of stacking fault is formed by simple slip of partial dislocations, presenting as the slight distortion of certain atomic layers without increasing or decreasing atoms. The  $I_2$  type of stacking fault, is formed by taking out a layer of atoms in the close-packed plane of (0001) and shifting the atoms above this layer with Burgers

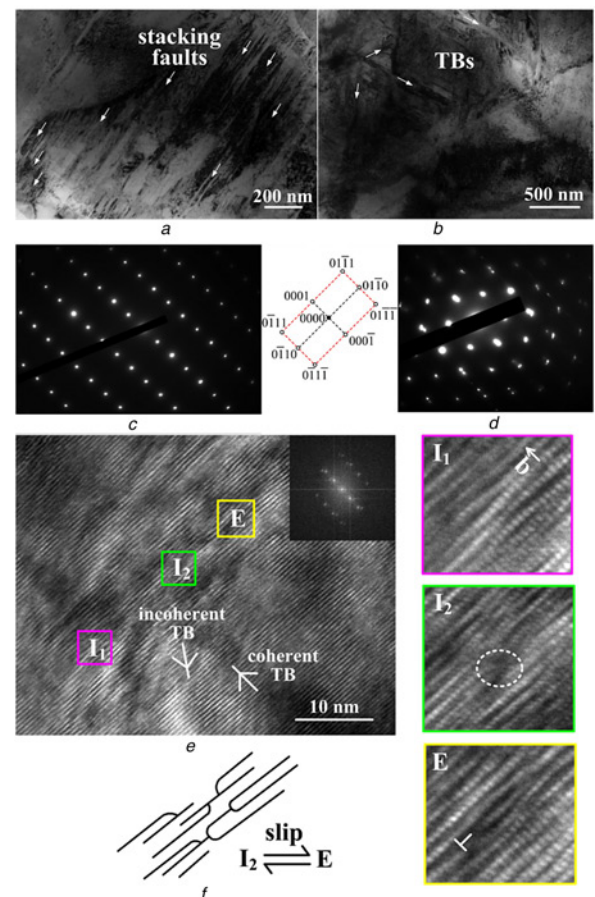


**Fig. 3** TEM bright field images at about 60  $\mu\text{m}$  below the topmost surface  
*c* is the corresponding SAED pattern picked in *a*  
*d* is the corresponding SAED pattern picked in *b*  
*e* is a high resolution TEM image; and  
*f* is a topological relationship diagram

vector  $\mathbf{b} = 1/3[-1100]$ . For the case of  $I_2$  outlined by green wire-frame, the region in white dashed circle is more likely induced by the collapse of vacancy cluster, which causes the formation of a Frank dislocation surrounding an epitaxy stacking fault in the way of  $1/2[0001] + 1/3[1100] + 1/3[\bar{1}100] \rightarrow 1/2[0001]$ . To reduce the system energy, a Shockley dislocation loop may be developed in this epitaxy stacking fault zone and transform this epitaxy stacking fault into an intrinsic stacking fault via its propagation in the way of  $1/3[\bar{1}100] + 1/2[0001] \rightarrow 1/6[\bar{2}203]$ . The  $E$  type of stacking fault is formed by inserting a layer of atoms between two normally stacking layers, like the case in Fig. 3e.

Obviously, the  $E$  type of stacking fault consumes the largest energy, hence existing with a least probability. But on the contrary, many epitaxy stacking faults are found in UIRP treated titanium alloy as well as intrinsic stacking faults. This is due to the feature of this surface nanocrystallisation technology. During UIRP, the ultrasonic impacting of processing head is intensively applied on a relatively small surface area, which in consequence generates large plastic strain energy with a very high plastic strain rate. Meanwhile, the plastic strain energy is also continuously provided by the rolling of processing head with constant force. The total supplied energy contributes to the formation of epitaxy stacking faults.

It is known that  $I_2$  and  $E$  can transmute into each other through slip. The actual atomic layers present a topological structure, schematically shown in Fig. 3f. Based on this mode, the three types of stacking faults could conveniently make conversion, thus promoting the generation, intersection of twins and the movement of

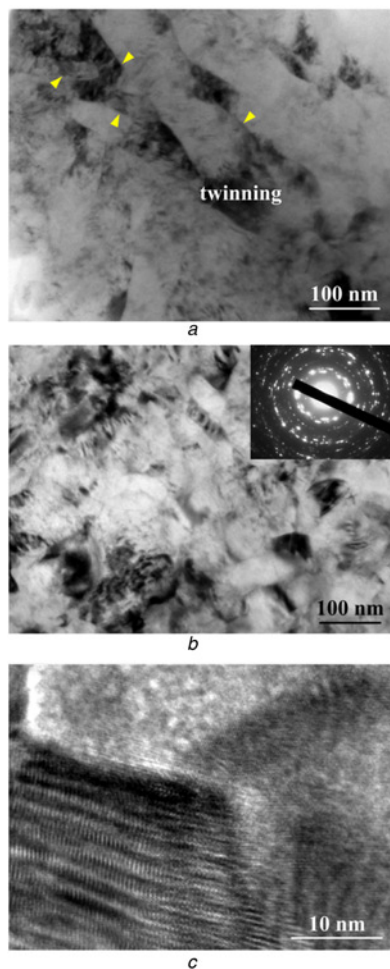


**Fig. 4** TEM bright field images and the corresponding SAED pattern at  
*a* About 30  $\mu\text{m}$  below the topmost surface and  
*b* Topmost surface  
*c* Is an HRTEM obtained in the topmost surface

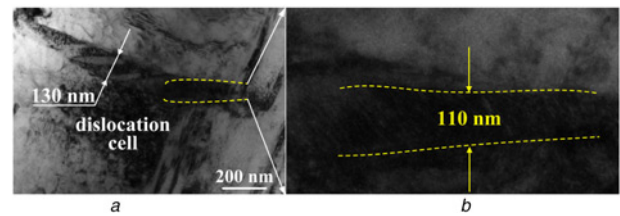


**Fig. 5** TEM images of  
*a* Beamlike secondary  $\alpha$ -phase and  
*b* Magnified lamellar secondary  $\alpha$ -phase

partial dislocations, as well as the interaction between twins and dislocations. As a result, the microstructure evolution can be easily realised. Moreover, both coherent twin boundaries and incoherent twin boundaries are found in the HRTEM image. Though the latter requires much more energy than the former, still many incoherent twin boundaries appear due to the dense topological structure.

During the late stage of surface nanocrystallisation, twinning is still active, which can be seen in Fig. 4a. As observed, in the depth of 30  $\mu\text{m}$  below the topmost surface, several twins appear in the bright field image, where secondary twins can also be found. Inside the twins and along the twin boundaries, there are high density dislocations. The width of twin bands is generally  $<100 \mu\text{m}$  and the length of twin bands is about 200–500  $\mu\text{m}$ , showing that the size of microstructure is decreased obviously. Fig. 4b shows the TEM image and corresponding SAED pattern of the topmost surface. It can be seen that grains in the topmost surface are mostly refined to 100 nm or  $<100 \text{ nm}$ . The diffraction spots in the SAED pattern basically form continuous rings, illustrating that the coarse grains become nano-grains with randomly crystallographic orientation. Fig. 4c shows the HRTEM image of the topmost surface. Clearly, grains present a hexagonal shape with the edge length of about 20 nm, demonstrating that the refined grains are equiaxed. The misorientation between adjacent grains is rather large. Twins are hardly found in the topmost surface, indicating that after grain size up to nano-scale, dislocation slip again becomes the governing mechanism of plastic deformation.

During UIRP, two types of secondary  $\alpha$ -phases were observed precipitating in  $\beta$ -substrate, as shown in Fig. 5. The beamlike secondary  $\alpha$ -phase with a width of 130 nm in Fig. 5a is martensitic  $\alpha'$  which is relatively independent with seldom mutual intervene. This is believed to reduce the dislocation slip resistance and contribute to improve the plasticity of alloy [13]. In close proximity to one end of the beamlike secondary  $\alpha$ -phase is the laminar secondary  $\alpha$ -phase with a width of 110 nm. The very narrow interlamellar spacing (only several nanometers) is considered to improve the elongation, thus acting a role similar like fine-grain strengthening.

**4. Conclusion:** The gradient crystalline evolution mechanism of as-received double-phase titanium alloy Ti-6.5Al-3.5Mo-1.5Zr-0.3Si during UIRP was investigated. It is found that in the early stage dislocation movement is quite active, and then deformation twinning becomes the dominant plastic deformation mechanism in a long period until grain size up to nano-scale. Due to the extremely high energy provided by combined effect of constant rolling and ultrasonic impacting, a surprisingly large amount of epitaxy stacking faults are generated despite the high energy they require. The actual atomic layers present a topological structure, which facilitates the conversion of intrinsic stacking faults and epitaxy stacking faults, the generation of twins, partial dislocations, and their intersection. After grains are refined to nano-scale, dislocation slip again becomes the main deformation mode. In addition, beamlike secondary  $\alpha$ -phase and laminar secondary  $\alpha$ -phase were observed precipitating in  $\beta$ -substrate, which could reduce the dislocation slip resistance and improve the elongation, thus contributing to improve the plasticity of alloy.

**5. Acknowledgments:** This work was supported by the National Science Foundation (grant no. 51405182) and the China Postdoctoral Science Foundation (grant no. 2014M561183).

## 6. References

- [1] Sun S.Y., Lv W.J.: 'Microstructure and mechanical properties of TC18 titanium alloy', *Rare. Metal. Mat. Eng.*, 2016, **45**, (5), pp. 1138–1141
- [2] Ahmed A.A., Mhaede M., Wollmann M., *ET AL.*: 'Effect of micro shot peening on the mechanical properties and corrosion behavior of two microstructure Ti–6Al–4V alloy', *Appl. Surf. Sci.*, 2016, **363**, pp. 50–58
- [3] Zhang X.H., Liu D.X.: 'Effect of shot peening on fretting fatigue of Ti811 alloy at elevated temperature', *Int. J. Fatigue*, 2009, **31**, (5), pp. 889–893
- [4] Foss B.J., Gray S., Hardy M.C., *ET AL.*: 'Analysis of shot-peening and residual stress relaxation in the nickel-based superalloy RR1000', *Acta. Mater.*, 2013, **61**, (7), pp. 2548–2559
- [5] Waltz L., Retraint D., Roos A., *ET AL.*: 'Combination of surface nano-crystallization and co-rolling: creating multilayer nanocrystalline composites', *Scripta. Mater.*, 2009, **60**, (1), pp. 21–24
- [6] Zhao X.H., Fan Y.J., Wang H.Y., *ET AL.*: 'Revealing the surface nano-enhancing mechanism of  $\alpha$ -titanium alloy by microstructure evolution', *Mater. Lett.*, 2015, **160**, pp. 51–54
- [7] Zhu K.Y., Vassel A., Brisset F., *ET AL.*: 'Nanostructure formation mechanism of  $\alpha$ -titanium using SMAT', *Acta. Mater.*, 2004, **52**, (14), pp. 4101–4110
- [8] Zhang F.C., Feng X.Y., Yang Z.N., *ET AL.*: 'Dislocation–twin boundary interactions induced nanocrystalline via SPD processing in bulk metals', *Sci. Rep.*, 2015, **5**, 8981
- [9] Wu X., Tao N., Hong Y., *ET AL.*: 'Strain-induced grain refinement of cobalt during surface mechanical attrition treatment', *Acta. Mater.*, 2005, **53**, (3), pp. 681–691
- [10] Thomas M., Jackson M.: 'The role of temperature and alloy chemistry on subsurface deformation mechanisms during shot peening of titanium alloys', *Scripta. Mater.*, 2012, **66**, (12), pp. 1065–1068
- [11] Liu Y., Wang L.J., Wang D.P.: 'Finite element modeling of ultrasonic surface rolling process', *J. Mater. Process. Tech.*, 2011, **211**, (12), pp. 2106–2113
- [12] Li H.M., Liu Y.G., Li M.Q., *ET AL.*: 'The gradient crystalline structure and microhardness in the treated layer of TC17 via high energy shot peening', *Appl. Surf. Sci.*, 2015, **357**, pp. 197–203
- [13] Li G.R., Li Y.M., Wang F.F., *ET AL.*: 'Microstructure and performance of solid TC4 titanium alloy subjected to the high pulsed magnetic field treatment', *J. Alloy. Compd.*, 2015, **644**, pp. 750–756